Detection of Sulfide Stress Cracking in a Supermartensitic Stainless Steel by Using Electrochemical Noise

C.J. Ortiz Alonso[1], M.A. Lucio–Garcia[1], I.A. Hermoso-Diaz[1], J.G. Chacon-Nava[2], A. MArtinez-Villafañe[2], J.G. Gonzalez-Rodriguez[1*]

[1] Universidad Autonoma del Estado de Morelos-CIICAP, Av. Universidad 1001, Col. Chamilpa, 62209-Cuernavaca, Mor., México
[2] Centro de Inv. En Materiales Avanzados, Miguel de Cervantes 108, Chihuahua, Chih., Mexico
*E-mail: ggonzalez@uaem.mx

An effort has been done to use electrochemical noise measurements in order to detect the nucleation and growth of cracks in a 13.5 Cr-4.7 Ni supermartensitic stainless steel in a H_2S-containing 3.5% NaCl solution. When the steel was immune to sulfide stress cracking (SSC), time series consisted of low intensity transients (lower than 60 nA/cm^2), without a regular frequency, due to strain-assisted metastable pit formation. However, when the steel was susceptible to SSC, time series consisted of periodic, high intensity transients (higher than 60 nA/cm^2) with a sudden increase and a slow recovery. Localization index increased during the straining, indicating the presence of localized events such as pits or cracks, regardless of the susceptibility of the steel to SSC. However, this index, by itself, could not distinguish between a pit or a crack. Noise resistance, on the other hand, decreased during the straining, due to the fact that more localized events such as pits or cracks occurred, with a slight increase towards the final rupture due to the re-passivation of the steel.

Keywords: sulfide stress cracking, stainless steel, electrochemical noise.

1. INTRODUCTION

The world demand for oil and gas is huge and does not show intent to decrease. [1] As a result, a great quantity of pipelines and oilfield equipment are required for the operation of oil and gas fields. However, the exposure of steels to hydrogen sulfide-containing environments makes the pipelines and oilfield equipment highly susceptible to sulfide stress corrosion cracking (SCC). [2-7] Typically, 13%Cr martensitic stainless steels and 22 or 25%Cr duplex stainless steels were used for sweet and slightly sour environments. The corrosion resistance of stainless steels increases with increasing the Cr content and other elements involved and stabilize the passive film (Mo, Ni, N, Cu, Co, Ti, W), giving rise to special alloys called Corrosion Resistance Alloy (CRA) - such as martensitic and

supermartensitic stainless steels [8]. Martensitic stainless steels have been increasingly applied in oil and gas application due to their good corrosion resistance and mechanical properties [9, 10]. Generally they are used in several corrosion conditions and when economical aspects are a critical issue, since they offer better mechanical and corrosion properties than carbon steels [11-14]. Electrochemical noise (EN), which is a non-destructive technique, consists of potential and current fluctuations spontaneously generated by corrosion reactions. EN technique has been increasingly used in field applications [15-19]. It has been extensively used to detect stress corrosion cracking susceptibility of steels, [20,21,23, 26] stainless steels, [22, 24,25, 30] brass, [18, 30] Al-alloys,[30], and Alloy 600 [28] in 3.5 NaCl [18,30], in $Na_2SO_4 + H_2SO_4$ [30], in boiling water reactor environments,[15,20,23], in ammonium nitrate + sodium nitrate environments, typical of nuclear waste environments [22], and in 25% Magnesium chloride boiling solution [17]. For instance, Ritter [15] carried out EN measurements on type 304 austenitic stainless steel during constant extension rate tensile tests in aqueous thiosulphate solution at room temperature to detect SCC. Similarly, Rathod [16] carried out stress corrosion cracking studies of aluminum alloys AA2219, AA8090, and AA5456 in heat-treated and non heat-treated condition using electrochemical noise technique with various applied stresses. Electrochemical noise time series data (corrosion potential vs. time) was obtained for the stressed tensile specimens in 3.5% NaCl aqueous solution at room temperature (27 ^{0}C). Similarly, Breimesser applied EN measurements to study the initiation and propagation of intergranular stress corrosion cracking in sensitized stainless steel under constant load. [17]. In all cases, current or potential fluctuations were related with the nucleation and propagation of stress corrosion cracks. Thus, the goal of this paper is to use EN measurements to detect SCC of a supermartensitic stainless steel in an H_2S-containing environment.

2. EXPERIMENTAL PROCEDURE

Table 1. Chemical composition of tested steel. (wt. %).

C	Mn	Si	Cr	Ni	Mo	S	P	Cu	N	Fe
0.02	0.75	0.3	13.5	4.7	1.7	0.0003	0.016	0.07	0.07	Bal.

Table 2. Mechanical propertie of tested steel.

YS (Ksi)	UTS (ksi)	Hardness (HRC)	% R.A.
99.2	126.1	26	60

Tested material included a supermartensitic stainless steel, UNS S41425, with chemical composition and mechanical properties as given in tables 1 and 2 respectively. Steel was austenitized at 932^{0}C during 60 min, air cooled, tempered at 611^{0}C during 11 hours and air cooled. Cylindrical tensile specimens with a 25.00 mm gauge length and 2.50 mm gauge diameter were machined. Before testing, the specimens were abraded longitudinally with 600-grade emery paper, degreased, and

masked, with the exception of the gauge length. Specimens were subjected to conventional, monotonic slow strain rate tensile (SSRT) at a strain rate of $1.00 \times 10^{-6} \text{ s}^{-1}$ at 25, 40, 60 and 80 ^{0}C in the testing solution which consisted of 3% NaCl solution, heated, deaerated with nitrogen gas. H_2S was produced by reacting 3.53 mg/l Sodium Sulfide (Na_2S) with 1.7 mg/l Acetic acid.. All the tests were done at the open circuit potential. The loss in ductility was assessed in terms of the percentage reduction in area (%R.A) by using:

$$\% R.A. = \frac{A_i - A_f}{A_i} x100 \qquad [1]$$

where A_i and A_f are the initial and final area respectively. A susceptibility index to SCC (I_{SCC}) was calculated as follows:

$$I_{SCC} = \frac{\% R.A._{air} - \% R.A._{NACE}}{\% R.A._{air}} \qquad [2]$$

where %R.A.$_{air}$ and %R.A.$_{NACE}$ are the percentage reduction in area values in air and in the H_2S-containing NACE solution respectively. The closer this index to 1, the higher the susceptibility to SCC.Tensile-fractured specimens were examined by a JEOL scanning electron microscope (SEM). Potentiodynamic polarization curves were performed at a sweep rate of 1 mV/s using a fully automated AC Gill potentiostat controlled with a desk top computer in the NACE solution and test temperatures. For these tests, a saturated calomel reference electrode (SCE) and a graphite auxiliary electrode were used. Polarization curves were performed once the free corrosion potential value (E_{corr}) was stable, i.e. it did not change in a 2 mV/min range. Corrosion current values, I_{corr}, were calculated by using Tafel extrapolation method.EN measurements in both current and potential were recorded during straining using as working electrode the tensile specimen and a nominally identical electrode as second working electrodes, and a reference SCE electrode. EN measurements were made recording the current fluctuations at a sampling rate of 1 point per second in blocks of 1024 readings. EN readings were taken every hour during the whole straining test. A fully automated zero resistance ammeter (ZRA) from ACM instruments was used in this case. Finally, the noise resistance, R_n, was then calculated as the ratio of the potential noise standard deviation, σ_v, over the current noise standard deviation, σ_i, according to Eq. [3]:

$$R_n = \sigma_v/\sigma_i \qquad [3]$$

Removal of the DC trend from the raw noise data was performed in the noise analysis. To accomplish this, a least square fitting method was used. An index called "Localization index", LI, was calculated as:

$$LI = \sigma_i / I_{rms} \qquad [4]$$

where σ_i is the current standard deviation and I_{rms} is the current root mean square value [31]. LI has been correlated with the tendency towards localized or uniform corrosion. For *LI* value*s* between 1

and 0.1, the alloy is highly susceptible to localized corrosion; for LI values between 0.01 and 0.001, the alloy is highly susceptible to uniform corrosion. Finally, for LI values between 0.1 and 0.01 the alloy is susceptible to a mixture of localized and uniform corrosion [31].

3. RESULTS AND DISCUSSION
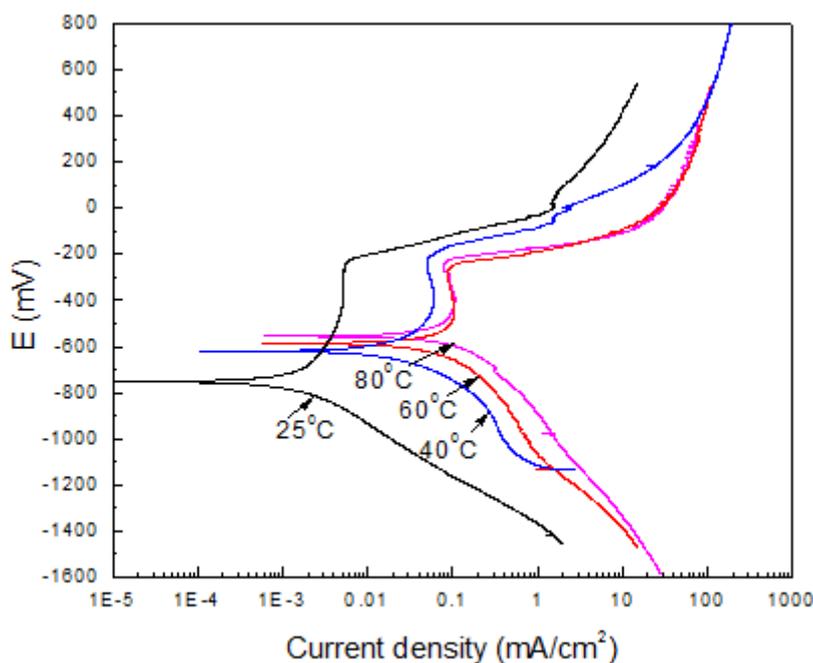
Figure 1. Effect of the temperature in the polarization curves for S41425 in a H$_2$S-containing 3.5% NaCl solution.

Polarization curves for the supermartensitic stainless steel in the H$_2$S-containing solution at different temperatures are shown in Fig. 1. It can be seen that the steel shows an active–passive behavior, with an E$_{corr}$ value shifting towards nobler values whereas the I$_{corr}$ value increased with an increase in the temperature. The passive behavior has been reported to be due to the formation of iron sulfide films on the metal surface [23, 33] which, under some H$_2$S concentrations are compact, adherent and protective. The passivation potential increases with the temperature, but the pitting potential remains more or less stable, making the passive region wider at 25^{0}C and it gets narrower as the temperature increases.

The different susceptibility values towards stress corrosion cracking for the different testing temperatures are given in table 3, which shows that the I$_{SCC}$ value increases with the temperature, i.e. the steel increases its susceptibility to SCC as the temperature increases, reaching a highest susceptibility at 80 ^{0}C.
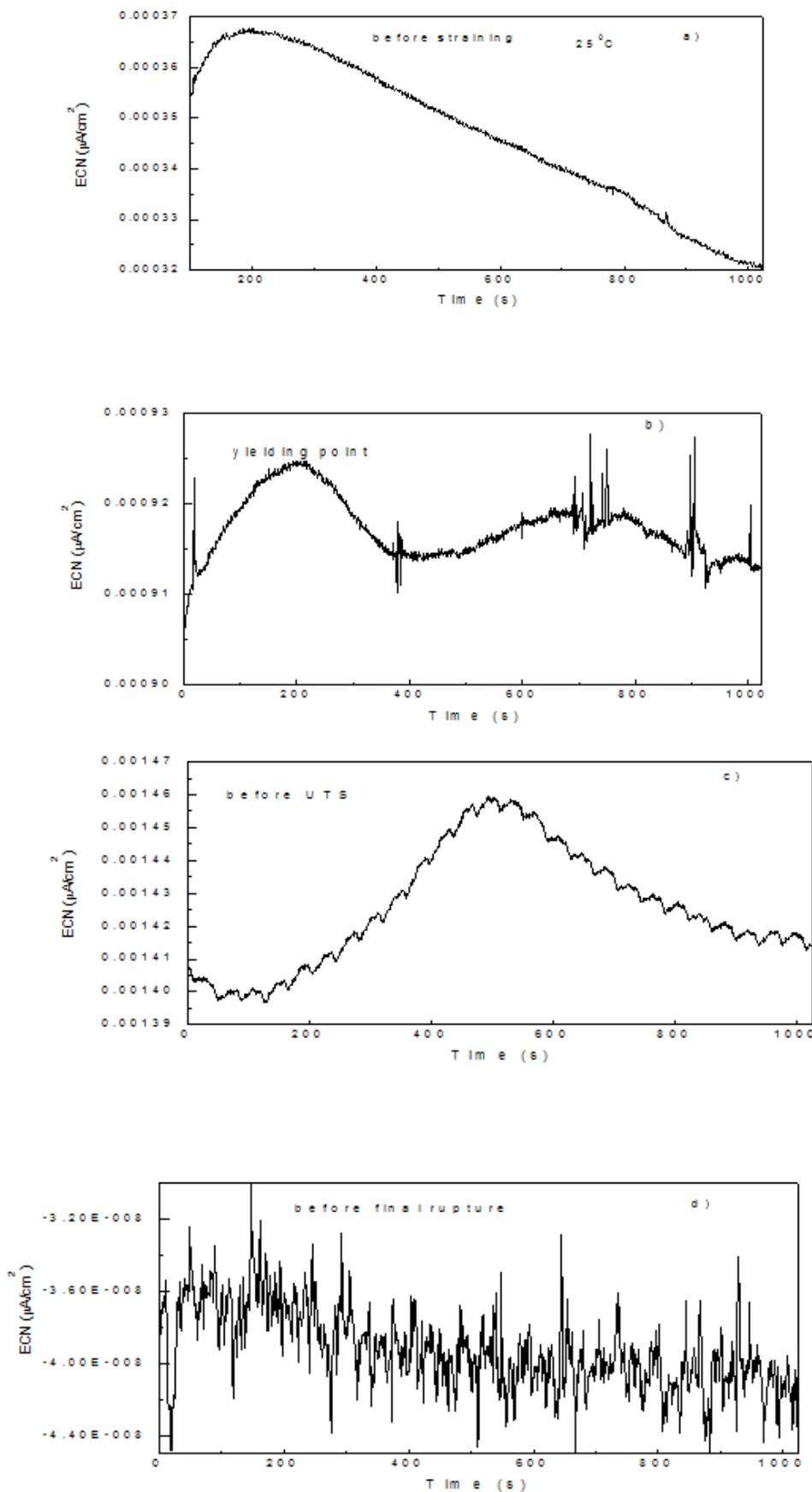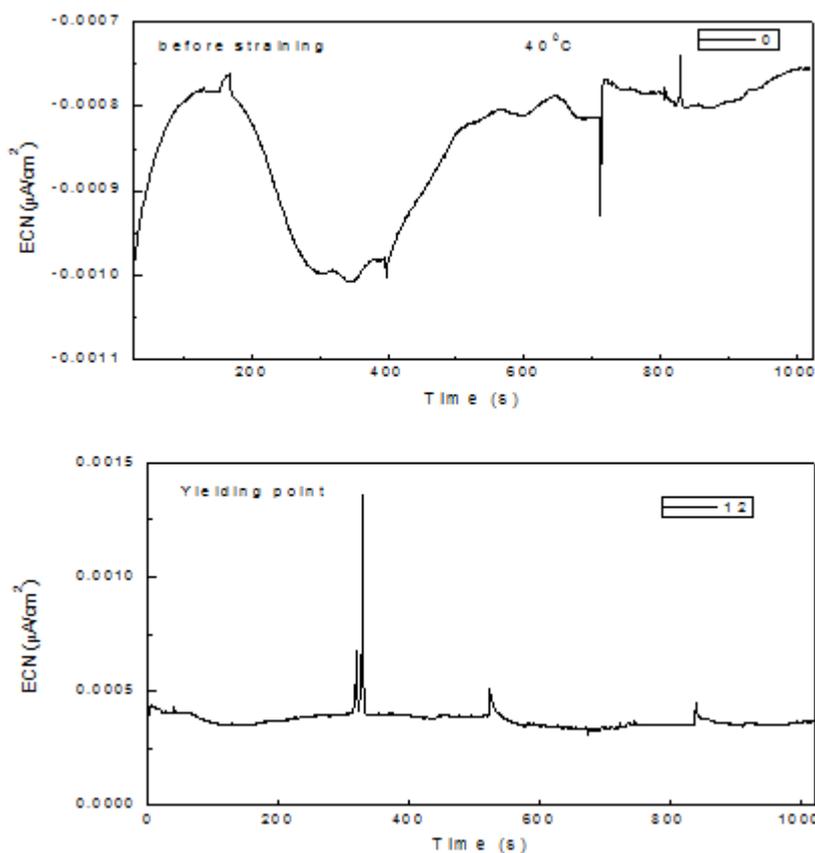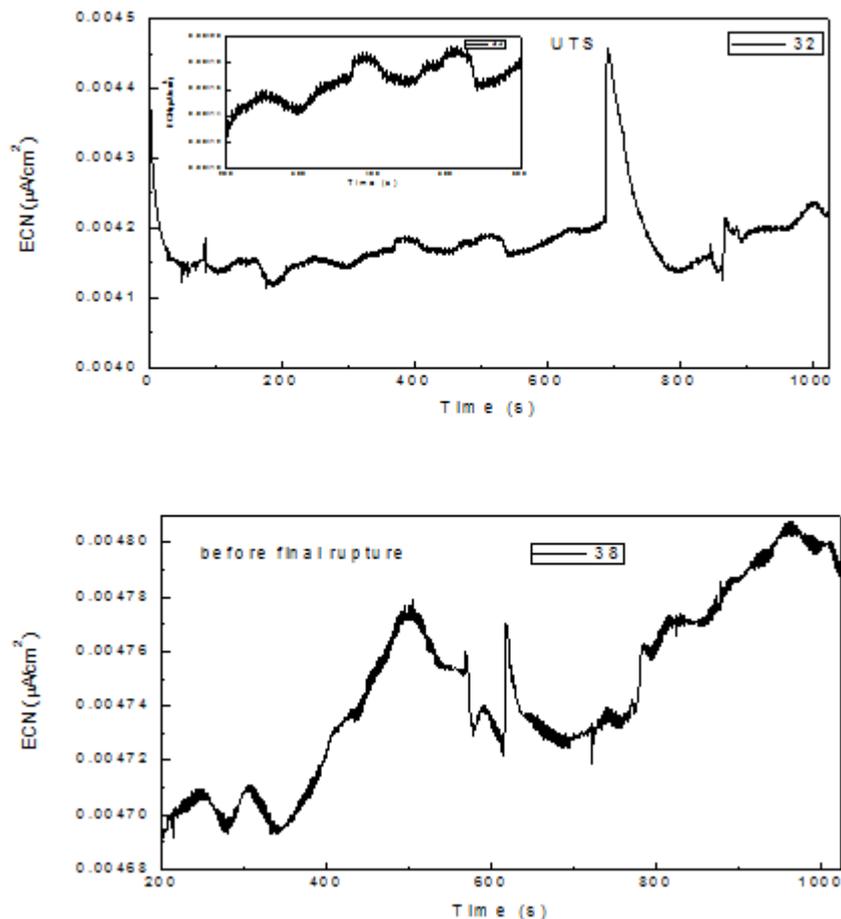
Figure 2. Noise in current for S41425 steel in the H_2S-containing 3.5% NaCl solution at 25 ^{0}C a)before straining, b) at the yielding pint, c) near the UTS and d) before final fracture.

Electrochemical current noise (ECN) time series for the specimen tested at 25 ^{0}C is shown in Fig. 2. This specimen was not susceptible to SCC. Before applying any stress, i.e. before straining, time series consisted of irregular (without a regular frequency), high frequency and low intensity transients, less than 1 nA/cm^2 indicating a passive state. Similar results were found Ritter for the sensitized 304 type stainless steel in thiosulfate solutions using the constant extension rate tensile tests when specimens were unloaded just after exceeding the nominal yield strength [15].

Once the straining begun, Fig. 2 b, a few transients with higher intensity than those found before straining were present, indicating, perhaps, the rupture of the passive film due to the straining. Uruchurtu and Dawson attributed these irregular current transients to the occurrence of breakdown and passivation processes occurring on the surface [32]. This could also be due to the strain-assisted dissolution or breakdown of the Cr_2O_3 layer and subsequent dissolution of the bare metal resulting in the formation of an environmentally compatible passive film. Before reaching the ultimatum tensile strength, UTS, Fig. 2 c, the transients did not change neither in intensity or frequency, but before reaching the final rupture, their intensity decreased considerably, Fig. 2 d, indicating that the pitting nucleation and growth has ended.

Time series for specimen strained at 40^{0}C is shown in Fig. 3. This specimen had an I_{SCC} value of 0.73, which indicates a low susceptibility to SCC of this steel in an H_2S-containing environment.
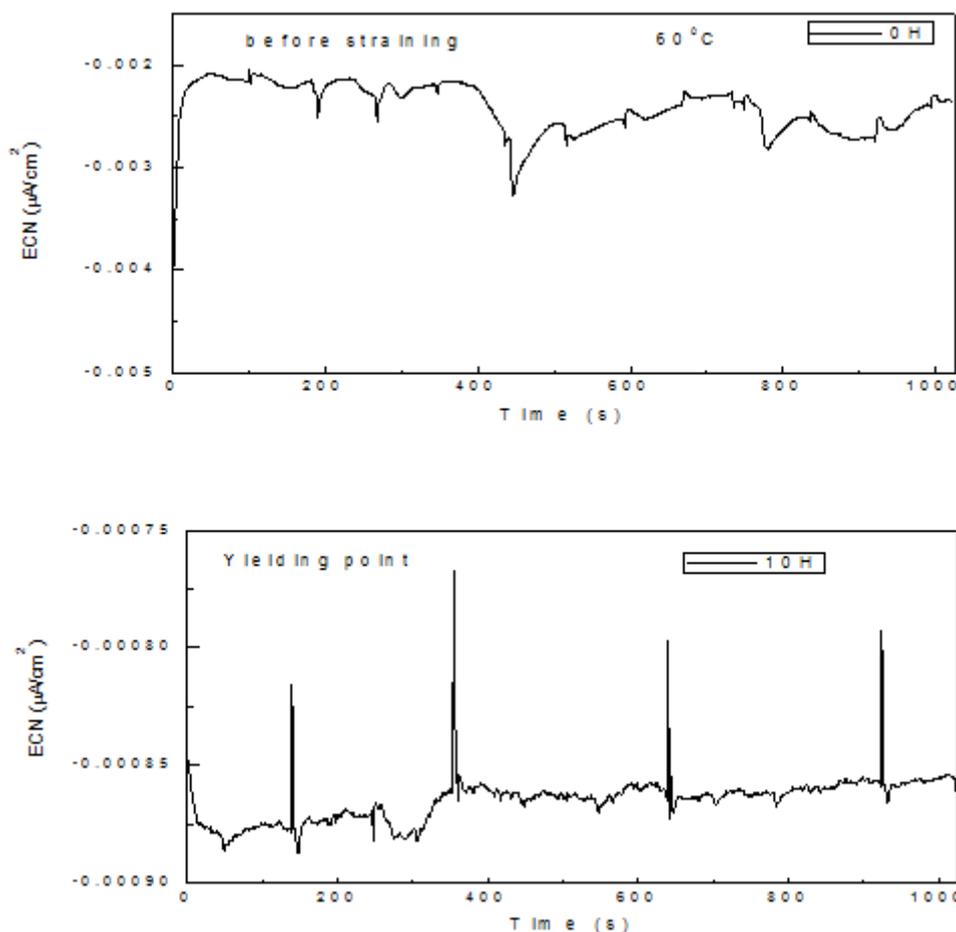
Figure 3. Noise in current for S41425 steel strained in the H_2S-containing 3.5% NaCl solution at 40 ^{0}C
a) before straining, b) at the yielding pint, c) near the UTS and d) before final fracture.

Before straining the steel or before reaching the yielding point, Fig. 3 a and b, time series show a few transients with intensities between 1-5 nA/cm^2, with a sudden increase in their intensity and a slow recovery, maybe due to a rupture of the passive layer due to the straining, and a re-healing of this layer. Every rise in current indicates dissolution of the material while the slow drop in current indicating re-passivation of the surface. When the test approached the UTS value and towards the final rupture of the specimen, Figs. 3 c and d, time series consisted of transients with an intensity lower than 1 nA/cm^2 but with very high frequency, in combination with a few transients with a sudden increase in their intensity in the anodic-going direction, and a slow recovery. The high frequency, low intensity transients are maybe due to passivation events of the steel, whereas the high intensity, low frequency transients are due to the rupture and re-healing of the passive layer due to the straining. It can be noted that for the tests carried out at 25 and 40^{0}C, the transients observed before straining or before reaching the yielding point, Fig. 2 a-b and Fig. 3 a-b, were random, showing the stochastic nature of pitting [34].

Table 3. Dependence of the I_{SCC} parameter as a function of the temperature

| T (^{0}C)	25	40	60	80
I_{SCC}	0.25	0.73	0.86	0.92

Specimen strained at 60 ^{0}C showed a big loss in ductility and therefore a high susceptibility to SCC since it had an I_{SCC} value of 0.86 as indicated in table 3. Before applying any stress, Fig. 4 a, the time series displayed some cathodic-going transients with an intensity lower than 1 nA/cm^2 may be due to some H$^+$ reduction reaction. However, around the yielding point, Fig. 4 b, the time series show some periodic, anodic-going transients, with a sudden increase in intensity, lower than 1 nA/cm^2, and a slow recovery. These transients are different to those observed at the yielding point at 25 and 40^{0}C. Once the yielding point was reached and the UTS is reached, Fig.4 c, the frequency and intensity of the anodic-going transients increase, with a sudden increase in their intensity and a slow recovery, to form a "tooth shape" signature. It can be seen that most of the current transients did not show a continuous decay of the current, but a small step towards the final phase of the transient. This type of transients was observed with further straining up to the final fracture of the steel, Fig. 4 d.
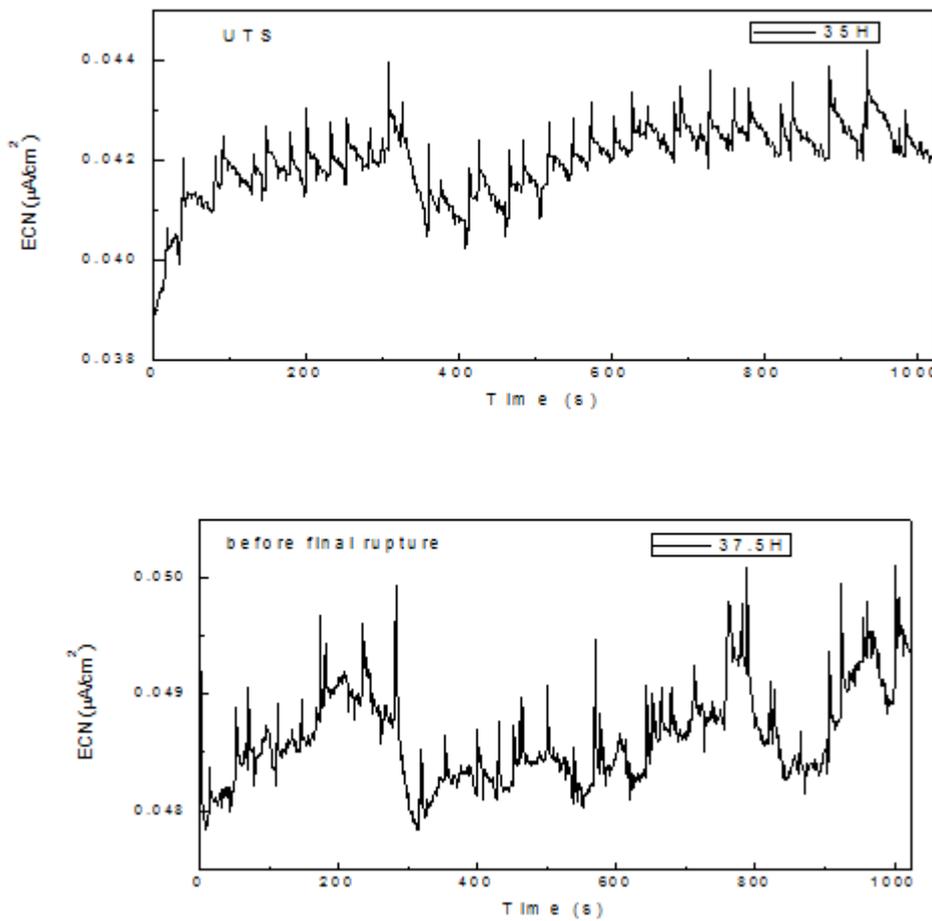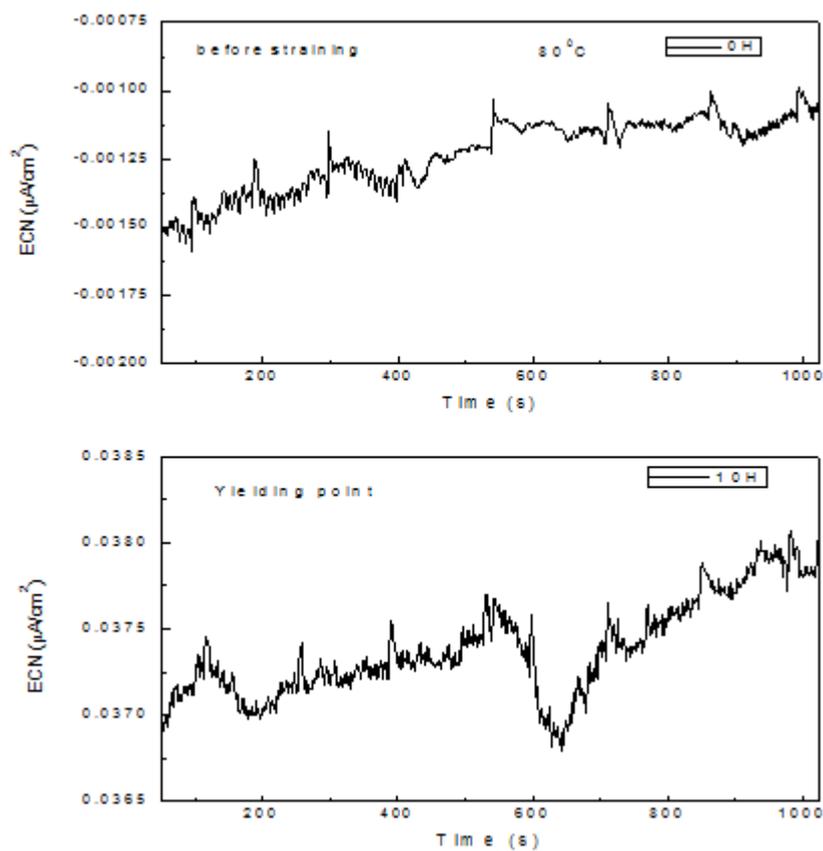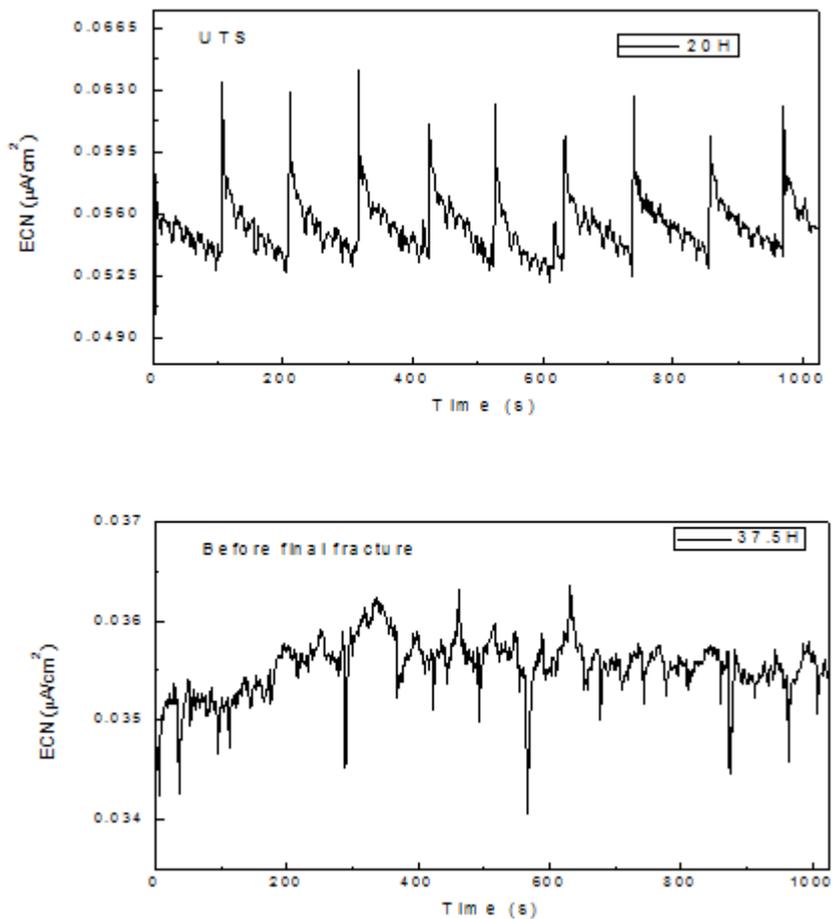
Figure 4. Noise in current for S41425 steel in strained in the H_2S-containing 3.5% NaCl solution at 60 ^{0}C a)before straining, b) at the yielding pint, c) near the UTS and d) before final fracture.

These transients have been observed during the SCC of some other materials [20-30] and they are related to the crack growth. The steep increase of the current transients in the noise signals, can be explained by rupture of the protective passive film on the stainless steel due to, for example dynamic plastic strain at the surface or crack-tip and subsequent anodic metal dissolution. This crack initiation process is then slowed down by repassivation, causing the decrease of the current. As soon as the crack tip and walls are fully repassivated, the metal dissolution is extremely limited and the current drops to its initial value. And the observed small step towards the final phase of the transient is due to rupture-repassivation events and the movement of the crack across individual grain boundaries [18]. An SEM micrograph of the fracture surface of this steel is shown in Fig. 5, which shows some intergranular cracks together with some quasi cleavage features, typical of a brittle type of fracture.
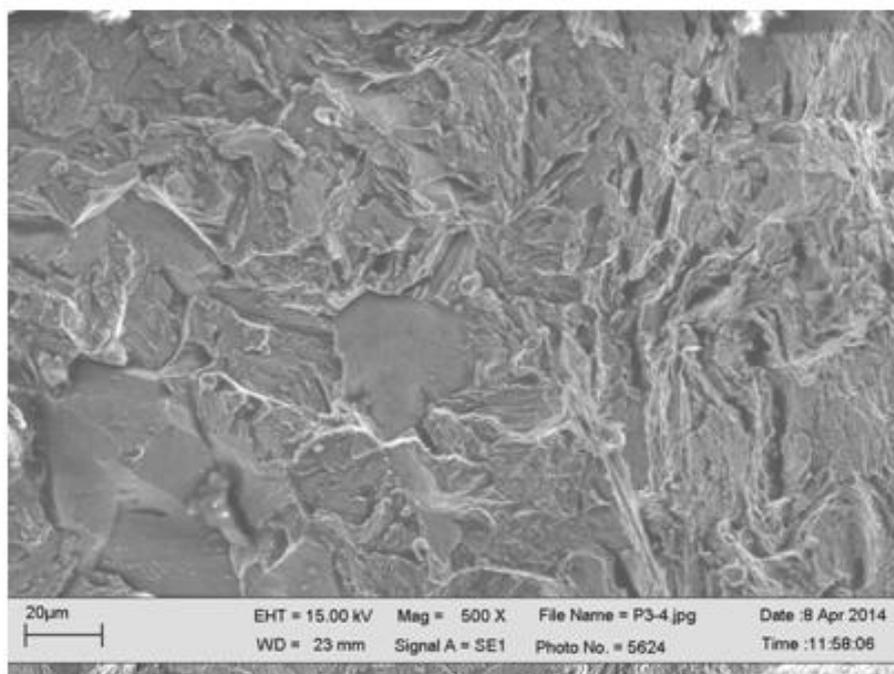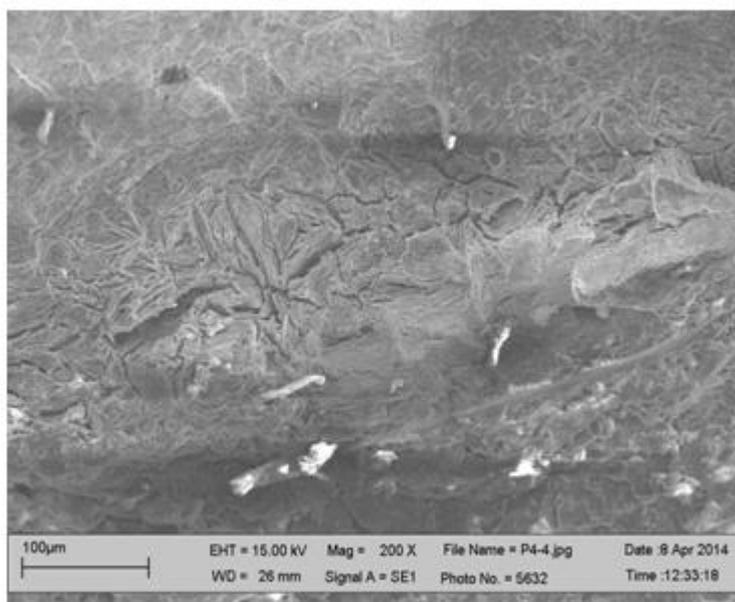
Figure 5. SEM micrograph of S41425 steel fractured in the H_2S-containing 3.5% NaCl solution at 60 ^{0}C

Figure 6. Noise in current for S41425 steel strained in the H_2S-containing 3.5% NaCl solution at 80 ^{0}C a) before straining, b) at the yielding pint, c) near the UTS and d) before final fracture.

Figure 7. SEM micrograph of S41425 steel fractured in the H_2S-containing 3.5% NaCl solution at 80 ^{0}C.

A similar behavior to the specimen strained at 60^0C was found for the test performed at 80^0C, Fig. 6. Before straining the steel or before reaching the yielding point, Figs. 6 a and b, only a few anodic-going transients were observed. However, once the UTS point was reached, Fig. 6 c, some periodic anodic-ongoing transients with intensity around 60 nA/cm^2 were observed. These transients showed a sudden increase in their intensity and a slow recovery, with a small step towards the final phase of the transient, due to the rupture of the protective passive film during straining, similar to those observed at the UTS point for the specimen strained at 60^0C. These types of transients were associated to the advance of short cracks by Stewart. [18] A micrograph of the fracture surface of this steel, Fig. 7, shows intergranular type of cracks with some evidence of anodic metal dissolution. Allam [35] investigating the SCC behavior of 72Cu–28Zn α-brass alloy in Na$_2$MoO$_4^-$, explained the found intergranular cracks for this alloy suggesting that preferential dissolution and mainly dezincification may take place at the pits and through the pores in air-formed film which enlarges with time and may lead an embrittled zone to crack fairly readily under a tensile load. Since grain boundaries are more active and dissolves at a much faster rate than the grain interior [36], i.e., the anodic sites are the grain boundaries while the grain interiors act as cathodic sites. These signal shapes can be explained by a series of overlapping events of film rupture, anodic dissolution and repassivation, according to the slip dissolution model for crack growth [37, 38].

Towards the end of the final fracture with a continuous straining, the anodic-ongoing transients disappeared and some cathodic–ongoing transients but with an intensity lower than 10 nA/cm^2 were observed. The burst type current signals disappeared or were of very low amplitude, thus indicating end of nucleation of stress corrosion cracks.

Breimesser [17], by applying electrochemical noise to monitor stress corrosion cracking of stainless steel in tetrathionate solution under constant load, concluded that large transients preceded by much smaller peaks and rising baseline currents, could be attributed to metastable pit formation and micro crack growth events of film rupture, anodic dissolution and repassivation. Therefore, in that case, transients exceeding 0.1 $\square$A/cm^2 and exhibiting high crack growth rates indicate the coalescence of micro cracks. Further growth and coalescence of the resulting cracks could then cause large fracture events [17]. Pits formed on stainless steel surfaces could either get repassivated before achieving stability or grow to become stable pits [37–38]. The phenomenon of metastable pitting is defined as the initiation of a single pit that gets repassivated immediately without growing further. Very similar results found Ritter for the same steel but in thiosulfate solutions using the constant extension rate tensile tests [15]. Thus, in our case, it seems that transients much smaller than 60 nA/cm^2 could be associated to the nucleation of pits, whereas transients with an intensity equal or higher than 60 nA/cm^2 are related to the formation of microcracks.

The variation of the Localization index value, LI, with time for the different tests is given in Fig. 8. We must say that difference in testing times is due to the different elongations, therefore, the specimen which did not show a susceptibility to SCC and had the lowest I$_{SCC}$ value, i.e. the specimen strained at 25 ^{0}C, had the longest time to failure also. Fig. 8 shows that in general terms, the LI value has a tendency to increase from values around 0.01 to values close to 1 before the specimen reaches the final rupture. This means that at the beginning of the test the steel was susceptible to a mixture of uniform and localized type of corrosion. However, as the straining continues, the susceptibility to

localized type of corrosion increases. This is because more localized type of corrosion events, such as pitting or cracks, are taking place.
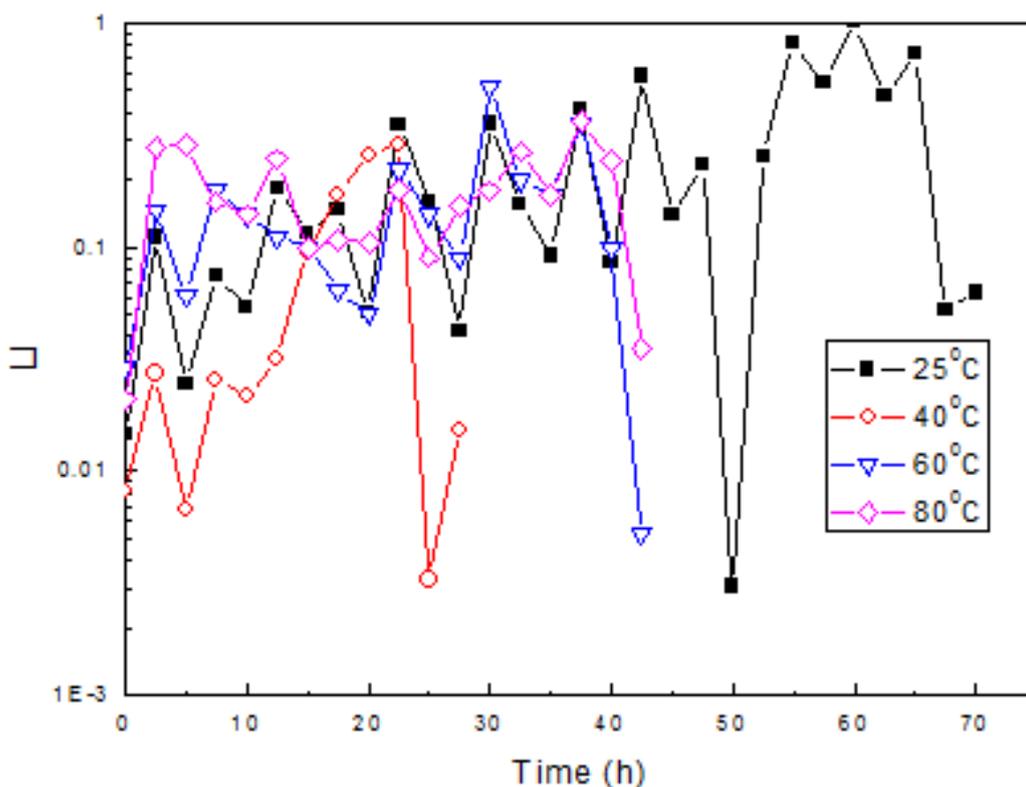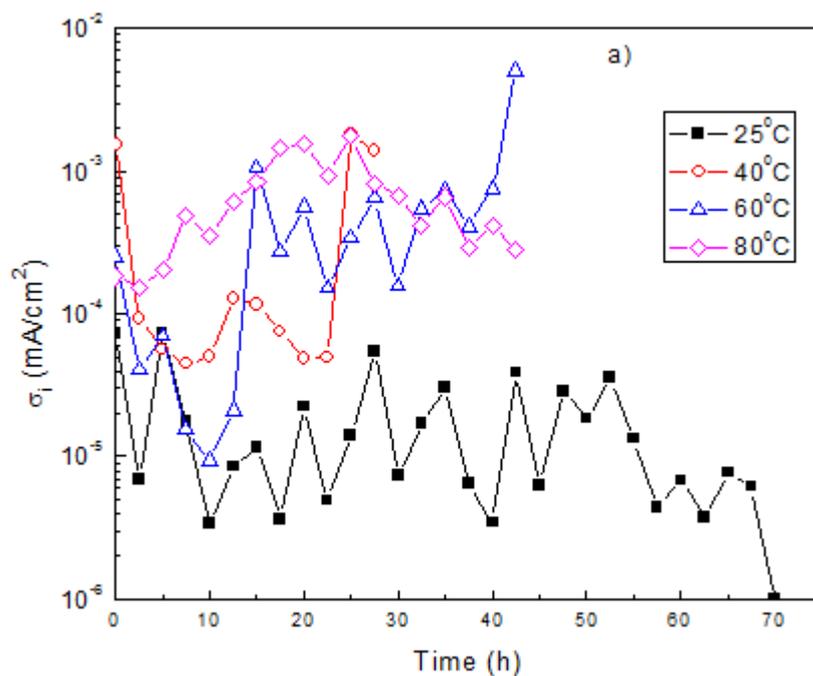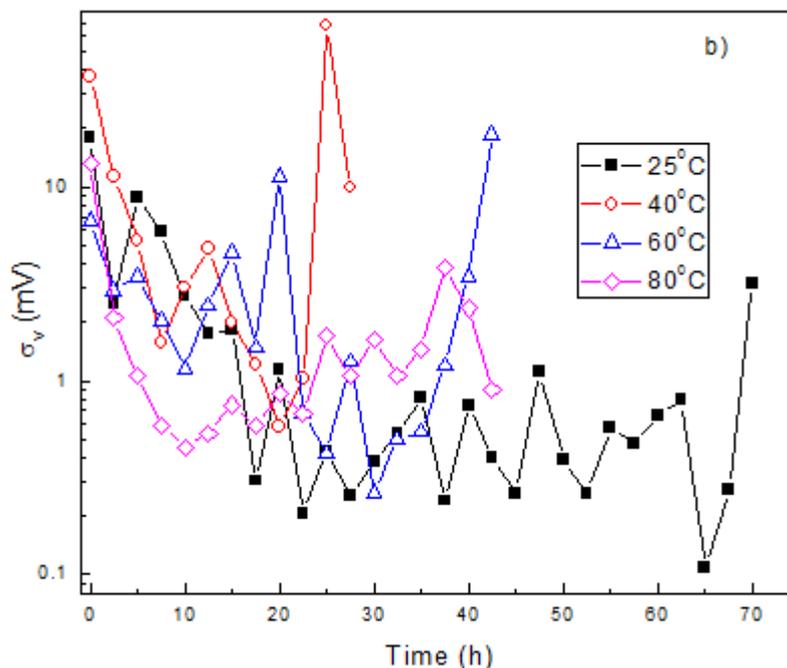

Figure 8. Variation of the localization index value, LI, with time for the different SSRT experiments.

Figure 9. Variation with time of the a) current noise standard deviation, σ_i and b) potential noise standard deviation values, σ_v, for the different SSRT experiments.

At the beginning of the straining, a few localized events such as pitting corrosion due to the passive layer disruption due to straining take place, but as the straining continues, especially once the yielding point has been reached, stress corrosion cracks start to appear and to grow. However, regardless of the testing temperature, the LI values sharply decreases just before the steel reaches the final rupture. This is because, just before reaching the final rupture, the crack grows so fast that the area inside the crack is passivated but,since now there is no straining, this passive film is not broken and protects the steel, so the IL decreases. As mentioned by Dawson [40] anodic transients can also be the results of metal dissolution at the crack wall and therefore, similar to pit initiation. In many cases therefore it is difficult to discriminate between anodic SCC, pitting and crevice corrosion.

Statistical parameters such as current noise standard deviation, σ_i and potential noise standard deviation, σ_v, at the different testing temperatures, are plotted in Fig. 9. It can be seen that the current noise standard deviation, σ_i, increases whereas the potential noise standard deviation, σ_v decreases by increasing both the testing temperature and the straining. The increase with the temperature means that the average intensity of the current transients increases due to an increase in the metal dissolution. The σ_i values at 25 ^{0}C had lowest values, due to the fact that this specimen was immune to SCC and only a few transients corresponding to the nucleation of pits were detected. The standard deviation values showed some oscillations, which could be correlated with the stress-assisted dissolution of the initially existing Cr_2O_3 film. The subsequent drop in the σ_i values could be attributed to the regeneration of environmental compatible passive film after dissolution. Following this drop, the σ_i and σ_v values oscillate between a maximum and a minimum. These oscillations could be associated with the continuous dissolution and re-passivation processes taking place during growth of the pit or crack. More or less a similar behavior exhibited by the current noise standard deviation, σ_i, was shown by the

noise resistance value, R_n, as shown in Fig. 10, where it can be seen that its value tends to decrease with time, i.e. an increase in the corrosion rate as time or straining elapses, but towards the end of the test, the R_n value increases.
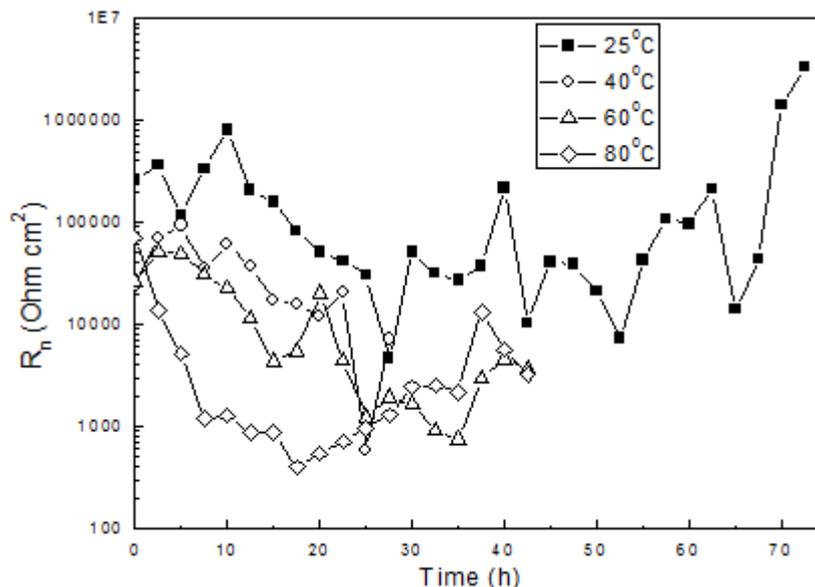
Figure 10. Variation of the noise resistance value, R_n, with time for the different SSRT experiments.

Additionally, the R_n value decreases as the testing temperature increased similar to the results reported by Girija et al. during the immersion of sensitized AISI type 304 SS in 4 N HNO_3 at 298, 323 and 348 K [41], i.e. the corrosion rate increases as the testing temperature increases. The increase in the corrosion rate with the testing temperature was observed in the polarization curves, Fig. 1, thus, there is agreement between the two different techniques. The fact that R_n decreases with time is due to the fact that more localized type of corrosion events, such as pits or cracks are taking place, and maybe close to the rupture of the passive layer inside the crack. If the model of anodic dissolution, as explained above, is the responsible for the crack growth, then the rupture of the passive layer and its repassivation are the responsible for the decrease in the R_n value. However, just before reaching the final rupture, the crack grows so fast that passive layer area inside the crack is not broken by the straining that the steel is protected, binging an increase in the R_n value.

4. CONCLUSIONS

A study of the detection of nucleation and growth of cracks in a 13.5 Cr-4.7 Ni supermartensitic stainless steel in a H_2S-containing 3.5% NaCl solution by using electrochemical noise measurements in current and potential. When the steel was immune to SSC, time series consisted of low intensity transients (lower than 60 nA/cm^2), without a regular frequency, due to straining-assisted

metastable pit formation. However, when the steel was susceptible to SSC, time series consisted of periodic, high intensity transients (higher than 60 nA/cm^2) due to the nucleation and growth of intergranular cracks. Localization index increased during the straining, indicating the presence of localized events such as pits or cracks regardless of the susceptibility of the steel to SSC. However, this index could not distinguish between pitting or crack nucleation and growth. On the other hand, the noise resistance value, R_n, decreased during the straining, with a increase towards the final rupture because the steel gets repassivated.

References

1. Trond Rogne, John M. Drugli and Ole Oystein Knudsen: "*Corrosion Performance of 13Cr Stainless Steels*", Corrosion 2000. Paper 152, NACE Conf. Div., P.O. Box 218340, Houston, Texas 77218-8340.
2. T. Taira, K. Tsukada, Y. Kobayashi, H. Inagaki, T. Watanabe, *Corrosion*, 37 (1981) 5.
3. H. Pircher, G. Sussek, *Corros. Sci.*, 27 (1987) 1183.
4. G. Domizzi, G. Anteri, J. Ovejero-Garcĺa, *Corros. Sci.,* 43 (2001) 325.
5. L.W. Tsay, M.Y. Chi, H.R. Chen, C. Chen, *Mater. Sci. Eng.,* 416 *A* (2006) 155.
6. M.C. Zhao, M. Liu, A. Atrens, Y.Y. Shan,K. Yang, *Mater. Sci. Eng.,* 478*A,* (2008) 43.
7. S. Ramadan, L. Gaillet, C. Tessier, H. Idrissi, *Appl. Surf. Sci.*, 254 (2008) 2255.
8. The Institute of Materials, *Corrosion Resistant Alloys for Oil and Gas Production: Guidance on General Requirements and Test Methods for H2S Service,* Maney publishing, 2002, 9.
9. H. Marchebois, J. Leyer, B. Orlans-Joliet, SCC performance of a Super 13 Cr Martensitic Stainless Steel for OCTG: Three-dimensional fitness-for-purpose mapping according to PH2S, pH and chloride content, NACE Corrosion conference (2007), Paper ISBN: 07090 2007 CP, Houston, TX, NACE International.
10. X. Li, T. Bell, *Corr. Sci*. 48 (2006) 2036.
11. M.D. Pereda, C.A. Gervasi, C.L. Llorente, P.D. Bilmes, *Corr. Sci*. 53 (2011) 3934.
12. H. Van-der-Winden, P. Toussaint, L. Coudreuse, Past, Present and Future of Weldable Supermartensitic Alloys, Supermartensitic Stainless Steel, Brussels, Belgium, 2002.
13. T.G. Gooch, P. Woollin, A.G. Haynes, Welding Metallurgy of Low Carbon 13% Chromium Martensitic Steels, Supermartensitic Stainless Steel, Brussels, Belgium, 1999.
14. D. Carrouge, Transformations in supermartensitic stainless steels, Ph.D. thesis, University of Cambridge, Department of Materials Science and Metallurgy, England, 2002.
15. S. Ritter, H. P. Seifert, *Materials and Corrosion* 64 (2013) 683.
16. R.C. Rathod, S.G. Sapate, R. Raman, W.S. Rathod, J. of Materials Engineering and Performance, 22 (2013) 3801.
17. Mathias Breimesser, Stefan Ritter, Hans-Peter Seifert, Thomas Suter, Sannakaisa Virtanen, Corr. Sci. 63 (2012) 129.
18. J. Stewart, D.B. Wells, P.M. Scott, *Corros. Sci*. 33 (1992) 73.
19. M.G. Pujar, N. Parvathavarthini, R.K. Dayal, S. Thirunavukkarasu, *Corros. Sci*. 51 (2009) 1707.
20. G.L. Edgemon, M.J. Danielson, G.E.C. Bell, *J. Nuclear Materials* 245 (1997) 201.
21. J. Hickling, D.F. Taylor, P.L. Andresen, *Materials and Corrosion* 49 (1998) 651.
22. J. Kovac, M. Leban, A. Legat, *Electrochim. Acta* 52 (2007) 7607.
23. T. Anita, M.G. Pujar, H. Shaikh, R.K. Dayal, H.S. Khatak, *Corros. Sci*. 48 (2006) 2689.
24. G. Du, J. Li, W.K. Wang, C. Jiang, S.Z. Song, *Corros. Sci*. 53 (2011) 2918.
25. S.W. Kim, H.P.Kim, *Corros. Sci*. 51 (2009) 191.
26. M. Leban, V. Dolecek, A. Legat, *Corrosion* 56 (2000)5 67.
27. J.L. Luo, L.J. Qiao, *Corrosion* 55 (1999) 765.

28. D. Eden, Corrosion´1998, National Association of Corrosion Engineers, Houston, TX, 1998, paper No. 386.

29. J. Kovac, C. Alaux, T. James Marrow, E. Govekar, A. Legat, *Corros. Sci.* 52 (2010) 2015.

30. Z. Shi, G. Song, Ch. Cao, H. Lin, M. Lu, *Electrochim. Acta*, 52 (2007) 2123.

31. I. A. AL-Zanki, J.S. Gill, J.L. Dawson, *Mater Sci Forum* 8(1986) 463.

32. J.C. Uruchurtu, J.L. Dawson, *Corrosion* 43 (1987) 19.

33. H. Ashassi-Sorkhabi, S.A. Nobavi-Amri, *Electrochim. Acta* 47 (2002) 2239.

34. Nageh K. Allam & Ahmed Abdel Nazeer,Elsayed A. Ashour, *J. Solid State Electrochem.*, 16 (2012) 353.

35. S.C. Sircar, U.K. Chatterjee, M. Zamin, H.G .Vijayendra, *Corros Sci* 12(1972) 217.

36. R.C. Newman, C. Healey, *Corros. Sci.* 49 (2007) 4040.

37. P.C. Pistorius, G.T. Burstein, Philosophical Transactions of the Royal Society (London) A 41 (1992) 531.

38. G.S. Frankel, L. Stockert, F. Hunkler, H. Bohni, *Corrosion* 43 (1987) 429.

39. J.L. Dawson, Electrochemical noise measurement. The definitive in-situ technique for corrosion applications? In: Kearns, J.R., Scully, J.R., Roberge, P.R., Reichert, D.L. Dawson, J.L. (eds.), Electrochemical Noise measurements for Corrosion Applications, STP 1277. ASTM, (1996) 3.

40. S. Girija, U. Kamachi Mudali, H.S. Khatak, Baldev Raj, *Corr. Sci.* 49 (2007) 4051.